接头形式对陶瓷/金属连接残余应力的影响

王 颖[1]， 何 鹏[1]， 冯吉才[1]， 张丽霞[1]， 顾小龙[2]， 王大勇[2]

（1. 哈尔滨工业大学 现代焊接生产技术国家重点实验室，哈尔滨 150001；
2. 浙江省冶金研究院 有限公司，杭州 310021）

王 颖

摘 要：采用有限元数值模拟方法研究了用 AgCuTi 钎料并添加 Kovar 中间层对氧化铝陶瓷/不锈钢进行钎焊连接接头残余应力的分布情况，分析接头形式对残余应力的影响。结果表明，采用等壁厚直接对接接头时，接头最大等效应力高达 600 MPa 以上，而将不锈钢壁厚减半后再进行对接时，接头最大等效应力可以降低近 200 MPa；两种情况下最大等效应力均出现在靠近连接界面的陶瓷中，断裂易在此位置发生。考查了各应力分量对最终残余应力的贡献，结果显示轴向应力和剪切应力在靠近界面的陶瓷侧有较大残余拉应力是造成接头强度降低的主要因素。

关键词：陶瓷/金属连接；残余应力；接头形式；有限元数值模拟
中图分类号：TG454 文献标识码：A 文章编号：0253－360X(2007)04－013－04

0 序 言

陶瓷/金属连接在电子、宇航、原子能、能源交通等部门得到广泛的应用[1, 2]。但由于陶瓷与金属的热膨胀系数与弹性模量等性能的不匹配，引起较大残余应力。尤其对于大尺寸构件，残余应力是影响连接强度的主要因素。因此，如何降低接头残余应力成为陶瓷/金属连接的主要研究内容之一[3－5]。而减小残余应力的措施主要有加入中间层，制定合理的工艺规范以及设计合理的接头形式几个方面。加入的中间层可以是热膨胀系数与陶瓷接近的合金，也可以是塑性良好的软质中间层，还可以加入兼具二者作用的多中间层，人们在这一方面投入了大量的精力。而接头形式对残余应力的影响研究的还并不深入。

作者主要研究接头形式对焊后残余应力的影响。陶瓷材料选用应用广泛的氧化铝陶瓷，金属材料则选用常见的不锈钢。在氧化铝陶瓷与不锈钢之间加入热膨胀系数与氧化铝陶瓷匹配的 Kovar 合金做中间层，在工艺方面采用了很小的冷却速度（5 ℃/min）。采用大型商用 MARC 有限元软件对接头残余应力分布进行模拟，以热弹塑性模型为基础，并考虑材料性能随温度的变化。

收稿日期：2006－05－22
基金项目：国家自然科学基金资助项目（50325517）

1 试验材料和方法

试验采用 95%Al_2O_3 陶瓷，1Cr18Ni9Ti 不锈钢，用活性钎料 AgCuTi 进行焊接，并加入热膨胀系数与氧化铝陶瓷匹配的 Kovar 合金 4J33 做中间层，图 1 为试件装配示意图。其中陶瓷、钎料、Kovar 合金均为外径 70 mm，内径 60 mm。而对于不锈钢则分别采用外径 70 mm，内径 60 mm，外径 70 mm，内径 65 mm 两种规格。陶瓷、不锈钢长度分别为 25，140 mm，钎料、Kovar 合金厚度分别为 0.1，0.3 mm。钎焊试验在真空炉中进行，真空度为 10^{-3} Pa。

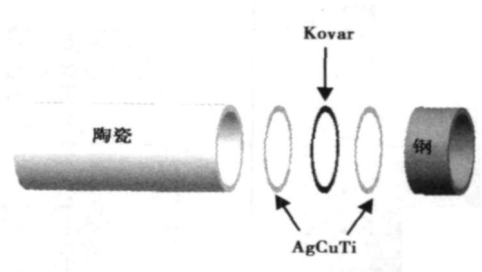

图 1 钎焊试件装配示意图

Fig. 1 Schematic drawing of alumina ceramic/steel brazing assembly

2 有限元模型

使用三维非线性有限元分析模型。根据对称性选取 1/4 进行计算，残余应力一般在界面附近

2～3 mm内取得最大值，因此对陶瓷和不锈钢各截取10 mm进行计算。分别采用等厚度直接对接（称为接头Ⅰ），以及将不锈钢壁厚尺寸减半对接（称为接头Ⅱ）两种模型进行比较分析。为保证计算精度同时减少计算时间，采用不均匀网格划分，在连接区域划分较细，其它区域则较粗，见图 2。

对氧化铝陶瓷选用线弹性模型，对 Kovar 合金、AgCuTi 钎料及不锈钢则选用弹塑性模型。考虑材料性能参数随温度的变化，计算中使用的材料参数值列于表 1[6－8]。在钎焊的升温过程中，材料处于自由状态，所以计算时不考虑升温过程，以钎料凝固温度 800 ℃为零应力温度。在从钎焊温度冷却至 800 ℃过程中，金属材料处于完全塑性状态，接头内不产生残余热应力。

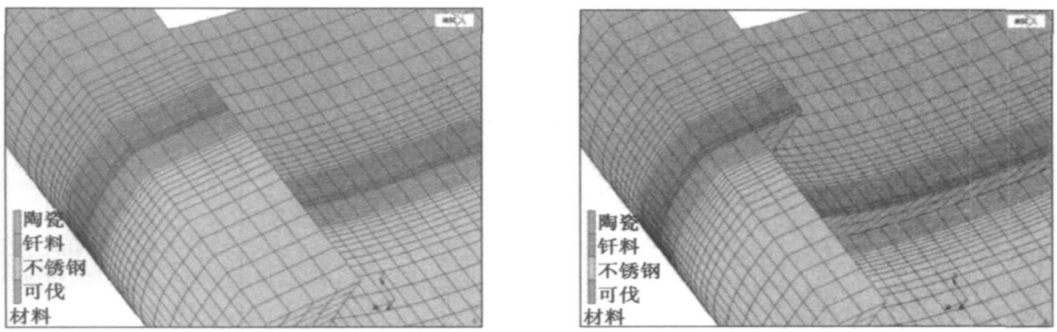

图 2 钎焊试件三维有限元网格

Fig. 2 Three-dimension finite element model of joints

表 1 有限元计算中所采用的材料参数

Table 1 Material parameters used in FEM calculation

材 料	温度 T/℃	弹性模量 E/GPa	热膨胀系数 α/(10^{-6} ℃$^{-1}$)	屈服强度 R_{eL}/MPa	泊松比
Al_2O_3 陶瓷	20～800	380	8	—	0.23
	20	93.6	19.0	230	
	200	85.0	19.7	170	
Ag—Cu—Ti	400	79.4	20.2	98	0.3
	600	70.2	20.5	25	
	800	58.1	21.0	20	
4J33	20～800	134	8.5	340	0.37
	20	196	10	275	
	200	182	12.5	196	
不锈钢	400	166	13.5	176	0.3
	600	150	14.5	157	
	800	147	18	98	

3 结果与讨论

3.1 有限元数值模拟结果

图 3 是两种接头等效应力分布云图。对比两图可以看出，采用直接对接的接头Ⅰ时，接头等效应力最高达到600 MPa以上，并且最大应力位于筒壁内侧。而将不锈钢壁厚减半后的接头中，等效应力最高值为 400 MPa 左右，与接头Ⅰ相比下降了近 200 MPa。同时，出现最大应力值位置转移到圆筒外侧。由于模型的对称性，等效应力沿圆周方向分布均匀，故以下重点考查等效应力沿轴向及径向的分布。图 4，图 5 分别是接头Ⅰ、接头Ⅱ中试件内表面和外表面等效应力沿轴向的变化曲线。

由图 4 可以看到，在接头Ⅰ中，不锈钢侧等效应力值稳定在 275 MPa 左右，并且内、外表面的等效应力值几乎相同。在不锈钢与钎料连接处，由于钎料屈服强度低，容易变形从而释放一部分应力，所以在该处应力值降低。而 Kovar 合金的屈服强度值较高，故 Kovar 合金与钎料界面应力值略有升高，从而出现在 0.5 mm 的钎料、Kovar 层内等效应力值上下波动的现象。在靠近界面 0.1 mm 的氧化铝陶瓷内，

等效应力取得最大值, 并且外表面的等效应力(442 MPa)要低于内表面(617 MPa)。对于陶瓷内表面来讲, 在 2 mm 高度范围内, 陶瓷内部的等效应力值均在400 MPa以上, 这对连接强度非常不利。

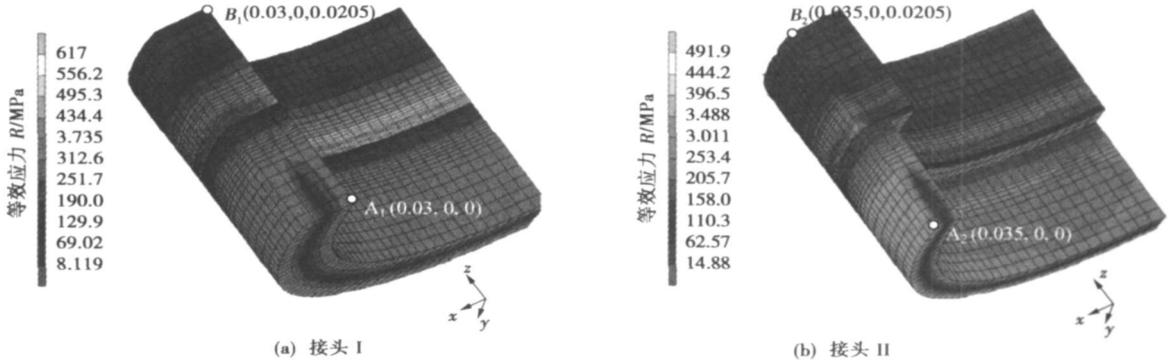

(a) 接头 I　　(b) 接头 II

图 3　接头等效应力分布云图

Fig. 3　Equivalent stress distribution of joints

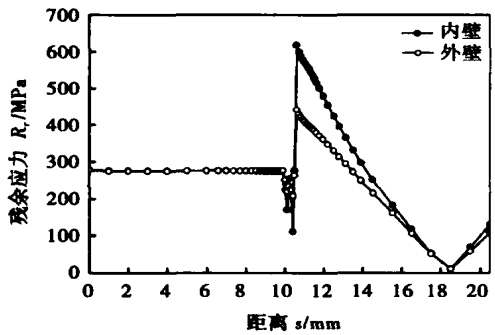

图 4　接头I 等效应力沿轴向的分布

Fig. 4　Distribution of equivalent stress along axial direction of joint Ⅰ

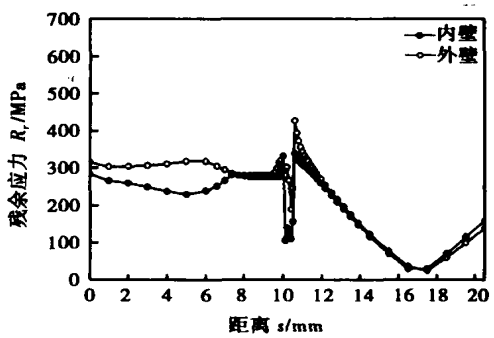

图 5　接头II 等效应力沿轴向的分布

Fig. 5　Distribution of equivalent stress along axial direction of joint Ⅱ

采用接头II时, 由于将不锈钢壁厚减半进行不等厚对接, 在形状变化的连接处不可避免地会产生应力集中, 这表现为在不锈钢与钎料内表面连接处等效应力不降反升的现象, 如图5 所示。同时, 也由于连接厚度的减小使得接头II中陶瓷内表面的最大等效应力降低了近 200 MPa, 而且靠近界面 2 mm 高度范围内的陶瓷中等效应力均大幅降低。对于外表面来讲, 接头等效应力与接头 I 相比大致相同。

在两种接头中, 等效应力均在靠近界面 0.1 mm 的氧化铝陶瓷内取得最大值, 因此考查该位置等效应力沿径向(由内到外)的变化, 结果如图 6 所示。可以看到采用接头 I 时, 等效应力在内表面最大为 617 MPa, 沿径向先逐渐降低, 在距内表面 3.75 mm 处有最小值为 414 MPa, 到外表面略有升高。而采用接头 II 时, 内表面等效应力降低到 321 MPa, 最大等效应力出现在外表面为 427 MPa, 在距内表面 2.5 mm处有最小值为 232 MPa。可见, 两种接头等效

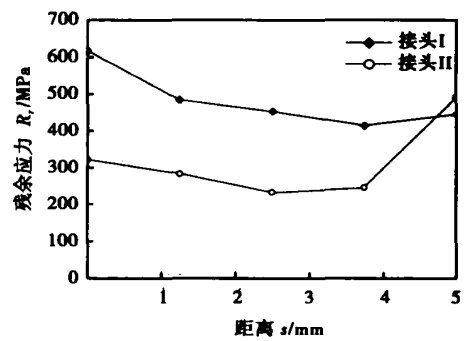

图 6　等效应力沿径向分布曲线

Fig. 6　Distribution of equivalent stress along radial direction

应力沿径向变化趋势不同, 采用接头 II时, 在接头最薄弱的位置(即靠近界面的陶瓷内), 等效应力得到有效降低。为考查各应力分量对最终残余应力的贡献, 在接头Ⅰ, 接头 II中分别选取两侧长 2 mm 的母

材,分析两种接头中各应力分量沿图 3 中 A_1B_1, A_2B_2 的变化,结果见图 7,图 8。选择这两个位置是因为 A_1B_1 和 A_2B_2 分别位于接头Ⅰ的内表面和接头Ⅱ的外表面,即接头中等效应力最大处,并且对于这两个位置 R_{xx} 即为径向应力,R_{yy} 则为周向应力。

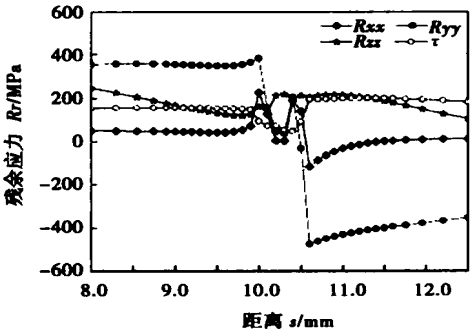

图 7 各应力分量沿 A_1B_1 的分布曲线

Fig. 7 Distribution of stresses along A_1B_1

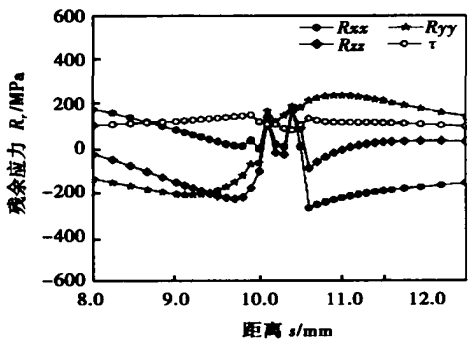

图 8 各应力分量沿 A_2B_2 的分布曲线

Fig. 8 Distribution of stresses along A_2B_2

由图 7 可以看到,周向应力和径向应力在钢侧均表现为拉应力,而在氧化铝陶瓷侧则表现为压应力。同时由于氧化铝陶瓷的抗压强度(2000 MPa)远远大于其抗拉强度(180 MPa),所以陶瓷该方向的压应力不会影响连接强度,而钢则可以通过塑性流动和高温蠕变等缓解应力集中。其中,径向应力的数值更小,对接头造成的不利影响更小。而 z 方向应力即轴向应力和剪切应力,在氧化铝陶瓷侧为拉应力,且在靠近界面的陶瓷处出现最大值,这对接头非常不利。采用接头Ⅱ时,各应力分量的分布趋势与接头Ⅰ大致相同,同时各应力分量数值均降低,如图 8 所示。因此,轴向应力和剪切应力是造成接头强度降低的主要因素。

3.2 钎焊试验结果

采用两种接头进行钎焊试验。结果发现,等壁厚直接对接时,试件缓慢冷却到室温后从真空炉中取出在氧化铝陶瓷侧发生开裂而无法得到完整的接头。而将不锈钢壁厚减半再进行对接时,由于接头残余应力大大降低,可以实现氧化铝陶瓷与不锈钢的连接,见图 9,验证了数值模拟结果的正确性。

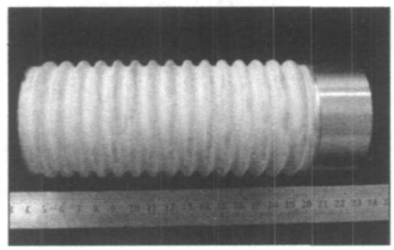

图 9 氧化铝陶瓷/不锈钢钎焊接头

Fig. 9 Brazed joint of alumina ceramic/steel

4 结 论

(1) 接头设计对于陶瓷金属连接非常重要,与等壁厚直接对接接头相比,将不锈钢壁厚减半,接头最大等效应力可以降低近 200 MPa。

(2) 在氧化铝陶瓷/不锈钢圆筒对接接头中,最大等效应力出现在靠近连接界面的陶瓷中,断裂易在此位置发生。

(3) 轴向应力和剪切应力在靠近界面的陶瓷侧有较大残余拉应力是造成接头强度降低的主要因素。

参考文献:

[1] 刘会杰, 冯吉才. 陶瓷与金属的连接方法与应用[J]. 焊接, 1999(6): 5—9.

[2] Matsuo Y, Ito M, Tanignch M. Ceramic-metal joining for automobiles [J]. Industrial Ceramics, 1999, 19(3): 203—207.

[3] Rabin Barry H, Williamson Richard L, Bruck Hugh A. Residual strains in an Al_2O_3—Ni joint bonded with a composite interlayer: experiments and FEM analysis[J]. J Am Ceram Soc, 1998, 81(6): 1541—1549.

[4] 熊柏青, 楚建新. 残余热应力对 Si_3N_4/金属钎焊接头性能的影响[J]. 中国有色金属学报, 1998, 8(2): 210—213.

[5] 程大勇, 陆善平, 郭 义. 陶瓷/金属钎焊金属内残余应力计算[J]. 材料研究学报, 2000, 14(增刊): 49—51.

[6] 膨胀合金组. 膨胀合金手册[M]. 北京: 冶金工业出版社, 1979.

[7] 机械工程材料性能数据手册组委会. 机械工程材料性能数据手册[M]. 北京: 机械工业出版社, 1994.

[8] 周 玉. 陶瓷材料学[M]. 哈尔滨: 哈尔滨工业大学出版社, 1995.

作者简介: 王 颖, 女, 1981 年出生, 博士研究生。主要从事陶瓷与金属连接方面的研究, 发表论文 2 篇。

Email: wishwangy@163.com

MAIN TOPICS, ABSTRACTS & KEY WORDS

Molten droplet size control in short-circuiting CO_2 arc welding

ZHU Zhiming, WU Wenkai, CHEN Qiang (Advanced Materials Processing Technology, Ministry of Education; Department of Mechanical Engineering, Tsinghua University, Beijing 100084, China). p1—4

Abstract: The formation process of molten droplet in shorting-circuit CO_2 arc welding and the influence of welding current on the molten droplet shape and short-circuiting transfer course were analyzed. After the welding current signals acquiring during the welding process being pretreated, an welding wire melting model for waveform controlled short-circuiting transfer welding was established by using the Least Square Method. Based on this model, an experimental research was carried out for the molten droplet size control by adjusting the width of welding pulse current in the initial phase of arc ignition to control the arc energy. The experimental results show that the molten droplet size increases monotonously as increasing the width of pulse current of arc ignition, which means that the arc energy and molten droplet size can be controlled effectively by changing the width of pulse current of arc ignition.

Key words: molten droplet size; welding wire melting model; molten droplet shape; short-circuiting course; pulse width control

Numerical simulation of hydrogen diffusion in low alloy steel welded joint under wet H_2S environment

GONG Jianming, JIANG Wenchun, TANG Jianqun, TU Shantong (College of Mechanical and Power Engineering, Nanjing University of Technology, Nanjing 210009, China). p5—8

Abstract: Hydrogen diffusion coefficients in weld metal, heat affected zone (HAZ) and base metal of the 16MnR low alloy steel welded joint were measured by electrochemical permeation technique. Based on finite element code-ABAQUS, the hydrogen diffusion in welded joint was numerically simulated. The effects of welding residual stress and microstructure on the hydrogen diffusion were taken into account. The variation of hydrogen concentration with time was obtained. The results show that the hydrogen diffusion coefficients and welding residual stress were much larger in weld metal and HAZ where the hydrogen accumulates, which can decrease the material properties and cause the cracking and damage related to hydrogen under wet H_2S environment.

Key words: welded joint; electrochemical permeation; hydrogen diffusion; numerical simulation

Numerical simulation on microdefect evaluation of diffusion bonded joints by resistance approach

XUAN Fuzhen, ZHANG Bo, LI Shuxin (School of Mechanical and Power Engineering, East China University of Science and Technology, Shanghai 200237, China). p9—12

Abstract: In terms of the morphology and characterization of interfacial microdefect of diffusion bonded joints, a two-dimension finite element model with the periodically distributed microdefects on the interface was presented. The influences of interfacial contact ratio, width and length of microdefects on increments of resistance were analyzed by applying the electromagnetic module in ANSYS software. Results indicated that there is a hyperbolic variation between the interfacial contact ratio and increment of resistance of diffusion bonded joints. The increment of resistance is affected by both width and length of interfacial microdefects. A higher sensitivity between the increment of resistance and interfacial microdefects was observed when the interfacial contact ratio was in 20%—80%. Based on the theoretical expression of contact ratio and increment of resistance proposed by Lodge et al, a modified equation was developed to accommodate the effects of size of interfacial microdefect, which can lead to a more precise evaluation for integrity of diffusion bonded joints.

Key words: diffusion bonding; microdefect; interfacial resistance; contact ratio; finite element method

Effect of joint types on residual stress in ceramic/metal joint

WANG Ying[1], HE Peng, FENG Jicai[1], ZHANG Lixia[1], GU Xiaolong[2], WANG Dayong[2] (1. National Key Laboratory of Advanced Welding Production Technology, Harbin Institute of Technology, Harbin 150001, China; 2. Zhejiang Metallurgical Research Institute Co., Ltd. Hangzhou 310021, China). p13—16

Abstract: By means of finite element numerical simulation, the effect of joint type on residual stress in ceramic/AgCuTi/Kovar/steel joint was investigated. The results show that in the direct butt joint the maximum residual stress is higher than 600 MPa. And halved the thickness of the steel cylinder, the residual stress of the joint can be reduced by 200 MPa compared with that in the direct butt joint. At both cases, the maximum residual stress value occurs on alumina ceramic near the brazing alloy/alumina ceramic interface. The fracture also occurs at this position. The radial stress and circumferential stress have little influence on the joints. And the axial stress and shear stress which have the peak tensile stress in alumina ceramic are the main factors which decrease the properties of the ceramic/metal joint.

Key words: ceramic/metal joint; residual stress; joint type;

finite element numerical simulation

Process of $(Cr, Fe)_7C_3$/γ — Fe ceramal composite coating formed by plasma surface metallurgy LIU Junbo (School of Mechanical and Electronic Engineering, Weifang University, Weifang 261061, Shandong, China). p17—20

Abstract: The effect of process parameters on the $(Cr, Fe)_7C_3$/γ—Fe ceramal composite coating formed by plasma surface metallurgy on Q235 steel substrate was researched. With the increase of scanning speed or decrease of working current, microstructure of coating was refined. Therefore, it can be ascertained that the optimum working current is 300 A and the optimum scanning speed is 500 mm/min. A in situ reinforcing phase $(Cr, Fe)_7C_3$ ceramal composite coating was fabricated on substrate of Q235 steel by plasma surface metallurgy with the Fe—Cr—C—Nb—Al alloy powders. The ceramal composite coating has a rapidly solidified microstructure consisted of primary $(Cr, Fe)_7C_3$ and the $(Cr, Fe)_7C_3$/γ—Fe eutectics, and is metallurgically bonded to Q235 steel substrate.

Key words: plasma surface metallurgy; process parameters; microstructure; microhardness

Medelling and simulation of resistance spot welding inverter JI Chuntao, PENG Xin, LUO Xianxing, DENG Lipeng (Material Science and Engineering School, Nanchang Institute of Aeronautical Technology, Nanchang 330034, China). p21—24

Abstract: The simulation tool in Matalab was used to characterize the resistance welding inverter system and to optimize the circuit parameters. The system output waveforms were analyzed and simulated for different filter capacitors and secondary loads. The result shows that the filter capacitor should be selected so that the rectifier output current is intermittent pulsative, and load current is supplied by the rectifier at voltage crest and by the capacitor at voltage trough. The secondary current rises as exponential fuction and its rising rate is a inverse proportional to the secondary inductance. It will finally reach a maximum value which is not affected by the inductance when provided the welding time is long enough.

Key words: resistance welding; inverter; system simulation

Microstructure and properties of welded joint for narrow gap laser welding of 42CrMo steel bevel gear shaft WU Shikai, YANG Wuxiong, DONG Peng, XIAO Rongshi (National Center of Laser Technology, Beijing University of Technology, Beijing 100022, China). p25—28

Abstract: The manufacturing of a heavy type bevel gear shaft is generally machined separately, and then jointed by welding. Aimed to the joining of the quenched and tempered 42CrMo steel bevel gear shafts for a heavy-duty machine, a 3500 W Slab CO_2 laser was applied and narrow gap laser welding process was adopted with filler wire of TGS—2CM. Meanwhile, the performance and metallographic structure of the joint were studied. The experiment results demonstrate that there are no cracks and porosities in the joint even without preheating and postweld heat treatment when the appropriate laser welding parameters are used. The microstructure in the weld and heat-affected zone is fine bainite. The micro-hardness of fusion area is about 580HV0.2, and no apparent softened zone exists in the welded joint. The tensile strength of the joint is in 980—1080 MPa, and equivalent to that of the base material, which is satisfied with the service demand.

Key words: laser welding; narrow gap; 42CrMo steel; bevel gear shaft; joint properties

A—TIG welding of magnesium alloy with activating welding wire LIU Liming, CAI Donghong, ZHANG Zhaodong, ZHU Meili (State Key Laboratory of Materials Modification & School of Materials Science and Engineering, Dalian University of Technology, Dalian 116024, China). p29—32, 37

Abstract: Several single common compounds were taken as basic activating fluxes in the tungsten inert gas (TIG) welding process with filler wire. The results indicated that in A—TIG welding of magnesium alley, the activating fluxes coated on the welding wire can also increase weld penetration. The chloride shows a prominent effect on the weld penetration, and the penetration even can be increased 3 times, which compared with the conventional TIG welding with filler wire. The boiling points of the fluxes that increased weld penetration are mostly in the regions about 900 ℃. The interfusion ability between the droplet metal and the weld pool metal became worse in the TIG welding process with filling activating welding wire than that with the normal wire, and filling ability of the welding wire deteriorates a little, comparing with the normal welding mire.

Key words: activating welding wire; activating fluxes; welding wire filling ability

Microstructure and wear-resisting property of TiC particle reinforced coatings cladded by TIG welding with multiple layer SONG Sili, ZOU Zengda, WANG Xinhong, LI Qingming (School of Materials Science and Engineering, Shandong University, Jinan 250061, China). p33—37

Abstract: By using TIG welding, ferrite based composite coating reinforced with TiC has been synthesized by preplaced alloy powder which contains Ti and C on the surface of conventional carbon steel. Results show that in situ TiC particles were prepared in the coating. The microstructure of the coating was mainly composed of ferrite, retained austenite, TiC particles and carbide. The surface hardness of the coating is higher than 55 HRC and presents gradient distribution nearer to the surface of the coating. The wear-resisting test indicated that the friction coefficient of the coating is varied acutely. Blocking effect of TiC particles leads to excellent wearing resistance. The coating has a excellent wear-resisting property. The